Effect of temperature on the microstructure and tensile properties of micro-crack free hastelloy X produced by selective laser melting

Maria L Montero-Sistiaga, Zhuangzhuang Liu, Ludo Bautmans, Steve Nardone, G Ji, Jean-Pierre Kruth, Jan van Humbeeck, Kim Vanmeensel

Journal Pre-proof

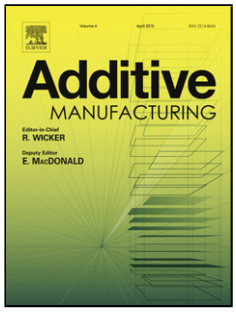

Effect of temperature on the microstructure and tensile properties of micro-crack free Hastelloy X produced by selective laser melting

Maria L. Montero-Sistiaga, Zhuangzhuang Liu, Ludo Bautmans, Steve Nardone, Gang Ji, Jean-Pierre Kruth, Jan Van Humbeeck, Kim Vanmeensel

PII: S2214-8604(19)30763-8

DOI: https://doi.org/10.1016/j.addma.2019.100995

Reference: ADDMA 100995

To appear in: *Additive Manufacturing*

Received Date: 29 June 2019

Revised Date: 12 November 2019

Accepted Date: 9 December 2019

Please cite this article as: Montero-Sistiaga ML, Liu Z, Bautmans L, Nardone S, Ji G, Kruth J-Pierre, Van Humbeeck J, Vanmeensel K, Effect of temperature on the microstructure and tensile properties of micro-crack free Hastelloy X produced by selective laser melting, *Additive Manufacturing* (2019), doi: https://doi.org/10.1016/j.addma.2019.100995

Effect of temperature on the microstructure and tensile properties of micro-crack free Hastelloy X produced by selective laser melting

Maria L. *Montero-Sistiaga* [ab], Zhuangzhuang *Liu* [a*], Ludo Bautmans [c], Steve *Nardone* [b], Gang *Ji* [d] Jean-Pierre *Kruth* [e], Jan *Van Humbeeck* [a] and Kim *Vanmeensel* [a]

[a] KU Leuven, Department of Materials Engineering, Kasteelpark Arenberg 44, Heverlee B-3001, Belgium.
[b] ENGIE Laborelec, Rodestraat 125, Linkebeek B1630, Belgium
[c] Oerlikon Eldim (NL) BV, AD Lomm 5943, The Netherlands
[d] Université de Lille, CNRS, INRA, ENSCL, UMR 8207 - UMET - Unité Matériaux et Transformations, F-59000 Lille, France
[e] KU Leuven, Department of Mechanical Engineering, Member of Flanders Make, Celestijnenlaan 300, B-3001, Heverlee, Belgium
[*]Corresponding author: zhuangzhuang.liu@kuleuven.be

Abstract

The high-temperature behaviour of micro-crack free Hastelloy X produced by SLM has been studied. The microstructure and mechanical behaviour of as-built parts and heat-treated (at 1177 and 800 °C) parts were investigated. Quasi-static tensile tests were performed at room temperature and elevated temperatures (650, 750 and 850 °C) for the three heat treatment conditions. In order to better understand the tensile test performance, the microstructure evolution of as-built samples as function of temperature was studied using confocal scanning laser microscopy (CSLM). CSLM allows in situ observation of the microstructure evolution while the sample temperature is increased. During tensile testing, a significant decrease in tensile strain was observed at a testing temperature of 750 °C that was attributed to the precipitation of carbides and Mo-rich intermetallic phases, as observed during

and after CSLM. The samples heated at 1177 °C showed less carbide formation due to their more homogeneous starting microstructure, which resulted in a tensile ductility increase as compared to the as-built and 800 °C heat-treated samples.

Key words: *Powder bed fusion, Selective laser melting, Hastelloy X, high temperature tensile test, microstructure evolution*

1 Introduction

Hastelloy X is a solid-solution strengthened nickel superalloy containing high amounts of Cr, Fe and Mo, as well as lower percentages of W and Co. It consists of a face centred cubic (fcc) phase that is stable up to high temperatures. This material is characterised by its excellent corrosion resistance and high-temperature strength. Given these properties, Hastelloy X is commonly used in gas turbines, combustion engines, aerospace and chemical processing applications [1–4].

Selective laser melting (SLM) or laser powder bed fusion (LPBF) is an additive manufacturing process which enables the fabrication of high-end and near-net-shape components in a layer-by-layer additive manner [5,6]. This process uses a highly focused laser beam to consolidate a metallic powder bed that results in very high cooling rates (around 10^7 K/s). Hence, a very fine cellular solidification morphology with limited segregation is obtained [7]. These high cooling rates also lead to residual stresses that can result in distortion and/or cracking of the parts [8,9]. Several nickel superalloys have been reported to be prone to cracking during SLM, such as IN738 [10,11], CM247LC [12–15] or even Hastelloy X [16–18].

The cracking problem of Hastelloy X produced by SLM has been investigated widely. Several works have reported on the influence of trace elements such as Si, Mn and C on the cracking susceptibility of the material when processed by SLM [17,19,20]. On the other hand, Harrison et al. [18] proposed increasing the amount of solid-solution strengthening

elements to increase the thermal shock resistance, hence reducing the crack susceptibility of Hastelloy X produced by SLM. Recently, Sanchez-Mata et al. [21] published the first work on the microstructure characterisation of commercial micro-crack free Hastelloy X produced by SLM. Those authors investigated the grain morphology in the as-built and heat-treated conditions.

Marchese et al. [22] investigated the effect of different heat treatments on the microstructure and phase formation of Hastelloy X samples with micro-cracks (2.60-3.32 mm/mm^2 crack density). In the as-built condition, the authors observed the presence of Mo-rich M_6C carbides within the interdendritic regions. It was suggested that the M_6C carbides formed either during solidification or during the in-process thermal cycles [20,22]. After hot isostatic pressing (HIP), both Mo-rich M_6C and Cr-rich $M_{23}C_6$ carbides formed at the grain boundaries and Mo-rich M_6C carbides were also observed within the grains. The authors performed a 6 h heat treatment at 750 °C in order to simulate the operational service temperature conditions of Hastelloy X. An overall increase in Cr-rich $M_{23}C_6$ carbides was observed after the heat treatment.

Tomus et al. [23] also investigated the influence of HIP and heat treatments on the room temperature tensile properties. In addition, the same authors [19] investigated the tensile behaviour at elevated temperatures (700 °C and 900 °C) of Hastelloy X. They observed a significant decrease in tensile strain with increasing temperature, especially for horizontal samples. A clear explanation, however, was not given in this publication.

Several research efforts have focused on the effect of different heat treatment temperatures on the phase formation and microstructure evolution in Hastelloy X. However, the evolution of the SLM microstructure with temperature and its effect on the high-temperature tensile

behaviour has not yet been reported. This information is a necessity to quantify the behaviour of SLM processed materials at operational temperatures.

Therefore, this work aims at broadening the knowledge on how the typical SLM hierarchical microstructure evolves with temperature and on understanding the elevated temperature tensile performance of SLM processed and micro-crack free Hastelloy X parts. Microstructural characterisation was performed on three samples: as-built, heat-treated at 1177 °C and heat-treated at 800 °C. Tensile tests at room and elevated temperatures were carried out on the three types of samples. In addition, confocal scanning laser microscopy (CSLM) was employed for in situ observation of the microstructure evolution during heating, shedding light on the interrelationship between the microstructure and tensile behaviour at elevated temperatures.

2 Material and methods

In this study, MetcoAdd HX-D powder, a modified commercial variant of Hastelloy X provided by Oerlikon AM, was used as feedstock material. The powder particles were spherical in shape and had a d_{50} value of 31.4 µm as seen in Figure 1. The chemical composition of the powder is shown in Table 1.

All samples were built using a SLM Solutions SLM280HL (Lübeck, Germany) machine. Several cube-shaped samples were built with varying parameters: laser power varying from 200 to 350 W, scan speed varying from 400 to 1200 mm/s, layer thickness from 30 to 50 µm and hatch spacing from 80 to 120 µm. The volumetric energy density was calculated as $E_v = P\,(h_s \cdot t \cdot v)^{-1}$ [J/mm^3] where P is the laser power (W), h_s is the hatch spacing (mm), t is the layer thickness (mm) and v is the scan speed (mm/s). Based on the process optimisation, the chosen optimal parameter combination equalled an energy density of 62.5 J/mm^3. The parts were built using a preheating temperature of 100 °C. The relative densities were measured

using the Archimedes method with a theoretical density of 8.39 g/cm^3, as measured by a helium pycnometer. 1 cm^3 cubes were built for microstructural investigation. Rectangular bars were built in horizontal and vertical directions (110×20×3 mm^3) and subsequently machined to dog-bone shaped specimens.

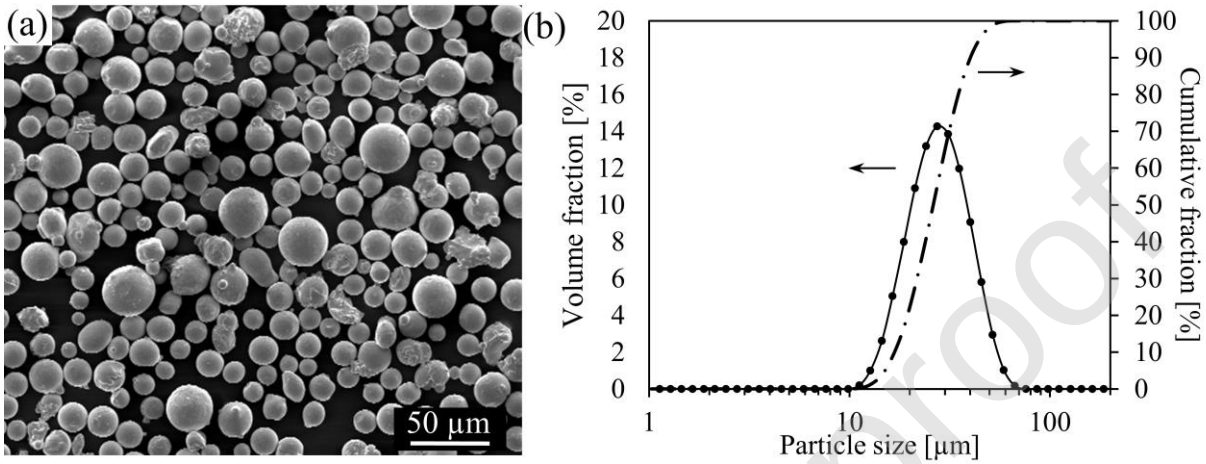

Figure 1(a) SEM image of powder morphology and (b) particle size distribution in volume and cumulative fraction.

Table 1. Composition of MetcoAdd HX-D powder used in weight percentage supplied by Oerlikon.

Weight Percent (nominal)							
Ni	**Cr**	**Fe**	**Mo**	**Co**	**W**	**C**	**Mn**
Balance	20.50-23.00	17-20	8-10	0.50-2.50	0.20-1.00	<0.15	< 1.00
Si	**Cu**	**Al**	**Ti**	**P**	**S**	**B**	
< 1.00	< 0.50	< 0.50	< 0.15	< 0.04	< 0.03	< 0.01	

The as-built (AB) cube-shaped samples were heat-treated in order to evaluate the microstructure evolution with temperature. Heat treatments were performed on the tensile samples at 1177 °C for 2 h (standard Hastelloy X heat treatment) and at 800 °C for 2 h followed by forced argon cooling at a rate of 40 °C/min, labelled as HT1 and HT2 respectively. The description of the three conditions is summarised in Table 2.

Table 2 Description of the three testing conditions: AB, HT1 and HT2.

	Condition
AB	As-built
HT1	2h at 1177 °C + argon cooling
HT2	2h at 800 °C + argon cooling

For microstructure evaluation, the samples were ground, polished with 3 and 1 µm diamond suspensions and then polished using an oxide polishing suspension (OPS). In order to reveal

the grain boundaries and the cellular structure, the polished samples were etched electrochemically using 10% oxalic acid solution at 7 V for 5 s. Light optical microscope (LOM) images were taken using a Keyence VHX-6000 microscope. A FEI Nova NanoSEM 450 was used to record electron micrographs using scanning electron microscopy (SEM). For high-resolution SEM images, the samples were analysed after OPS polishing to avoid preferential etching of the precipitates. Electron backscattered diffraction (EBSD) scans were performed using a step size of 1.5 µm.

Tensile tests were performed at room temperature (RT), 650 °C, 750 °C and 850 °C. The tensile samples were machined to a dog-bone shape having a nominal width of 7 mm, thickness of 3 mm and gauge length of 25 mm. A heating rate of 10 °C/min and 30 minutes of dwell time at the testing temperature were applied before each tensile test in order to homogenise the sample temperature. The room temperature samples were tested according to the ASTM E8 norm, at a strain rate of 0.015 strain/min up to the yield point and at a strain rate of 0.4 strain/min during the rest of the loading curve. Strain rates were applied and recorded over the gauge length. The elevated temperature tests were performed according to the ASTM E21-17 norm, at a strain rate of 0.005 strain/min up to the yield point and at a strain rate of 0.05 strain/min during the rest of the loading curve. After testing, the samples were air cooled. For all tests, an extensometer was just up to the yield point and after, displacement was recorded by the cross-head displacement.

A confocal scanning laser microscope (CSLM), equipped with a hot stage up to 1750 °C, was used to investigate the microstructure evolution. Cylindrical samples (diameter: 4 mm and height: 3 mm) were machined from cubes. The circular cross sections (parallel to the building direction, XZ plane) were polished and etched using oxalic acid and later investigated by CSLM. The samples were heated to 750 and 850 °C and the temperature was maintained for 40 minutes in order to mimic the thermal conditions of the tensile tests at elevated

temperatures. The heating rate was 10 °C/min and the cooling rate was about 375 °C/min down to 300 °C and 90 °C/min between 300 °C and room temperature. Before heating, the furnace chamber was first evacuated to ca. 10 Pa and then purged with pure argon gas for three times to eliminate the residual oxygen in the furnace. The furnace chamber was then refilled with argon to ensure that the experiments were performed under a deoxidised argon atmosphere in order to avoid any oxidation. Light optical images were recorded at a sampling frequency of 1 Hz during the whole heating and cooling cycle.

Transmission electron microscopy (TEM) specimens of 3 mm in diameter were prepared by mechanical polishing and final ion milling in a GATAN precision ion polishing system. A FEI Tecnai G2 twin microscope, operated at 200 kV and equipped with an Oxford energy dispersive X-ray (EDX) spectrometry system, was used for TEM characterisation.

3 Results

3.1 SLM process optimisation and microstructural characterisation of as-built samples

Cubes were built with different scanning parameters in order to optimise the sample density and reduce the crack density. The relative density of all samples is shown in Figure 2 as a function of the volumetric energy density. None of the samples showed cracks, contrary to earlier experiments performed with a different powder [7]. When increasing the volumetric energy density, the relative density increases exponentially up to 50 J/mm^3, resulting in 99% dense parts. As seen in the bottom inset micrograph, low energy densities result in lack of fusion porosities and, hence low relative densities. Above 50 J/mm^3 high relative densities are obtained. No relative density decrease is observed as seen previously for similar alloys where keyhole porosities are formed at an energy density of 75 J/mm^3 [7]. The two top inset micrographs show the high-density parts obtained at different energy density levels ranging from 75-150 J/mm^3, with the absence of pores.

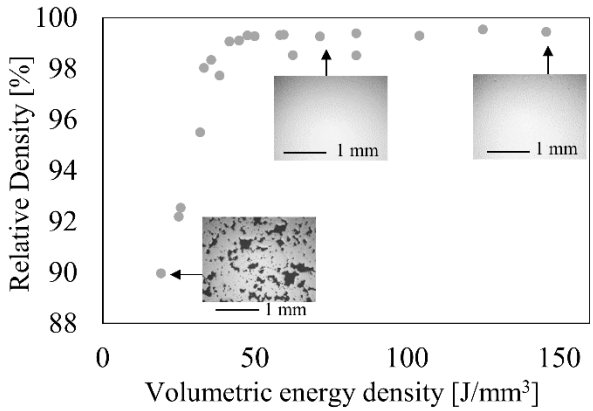

Figure 2 Relative density of cubes as a function of the volumetric energy. The top images show full dense samples while the bottom micrograph shows unmolten regions in black.

Figure 3 (a-b) shows the microstructure of the samples produced with this energy density. In Figure 3 (a), a polished cross-section is shown indicating a fully dense microstructure without remnant porosity nor cracks. After etching, a typical SLM microstructure (Figure 3 (b)) is observed, showing hemispherical melt-pools and the absence of micro-cracks is confirmed. Using this powder, shallow and wide melt-pools are observed. This melt-pools enhance epitaxial growth of elongated grains, often several hundreds of microns in size, along the building direction (XZ plane) as also seen in the EBSD image in Figure 3 (c). Figure 3 (d) shows that the grains have a cross-sectional diameter of 60-70 µm (YZ plane). Considering the high aspect ratio of the epitaxially grown grains, anisotropic mechanical properties can be expected.

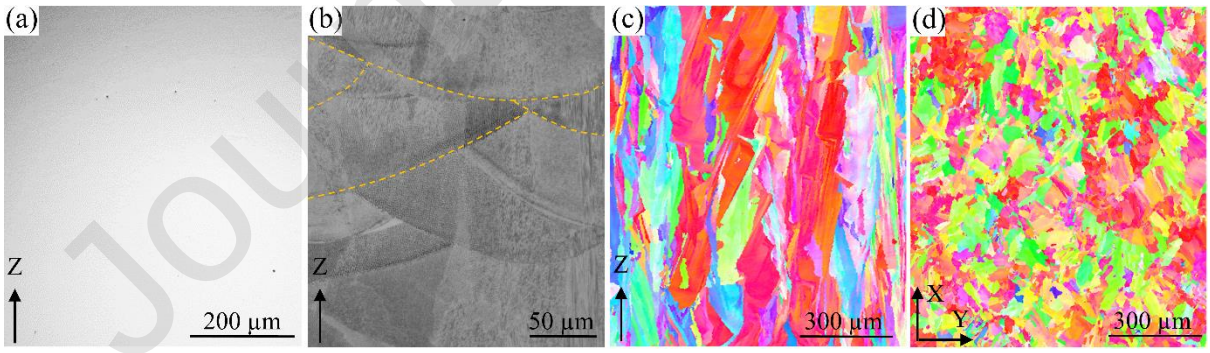

Figure 3 Microstructure of AB Hastelloy X part produced by SLM. (a) polished cross section along the building direction (Z), (b) etched microstructure along the building direction (Z), (c) EBSD pattern collected from a XZ plane and (d) EBSD pattern collected from a XY plane.

At sub-grain level (Figure 4), a cellular solidification morphology is observed with cell diameters below 1 µm. Cells tend to grow along and opposite to the direction of the highest thermal gradient. Therefore, in a polished cross-section, some grains contain cells with

elongated shape while others show the cross-sections of cells with a cylindrical shape. Figure 4 shows both the sub-grains that were cross-sectioned parallel and perpendicular to their growth direction. The latter is highlighted in blue in Figure 4(a-b). Figure 4(a) originates from a sample surface that was etched after polishing, while Figure 4(b) shows a sample surface that was only polished using OPS. When the samples are not etched, no melt-pool structure is observed and only the different cell morphologies inside the grains can be seen. The contrast difference between the different cells within one grain, as observed in the micrographs of the unetched sample surface, is related to preferential etching during the OPS polishing step. On the other hand, Figure 4 (c-d) shows the zoomed regions for the two cellular solidification morphologies. Note that the nanometre-sized grey spots originate from the OPS polishing step. They are silica particles as confirmed by EDS. The black nanometre-sized phases are believed to be Ti-Al-Si-O rich phases, as reported previously in [24].

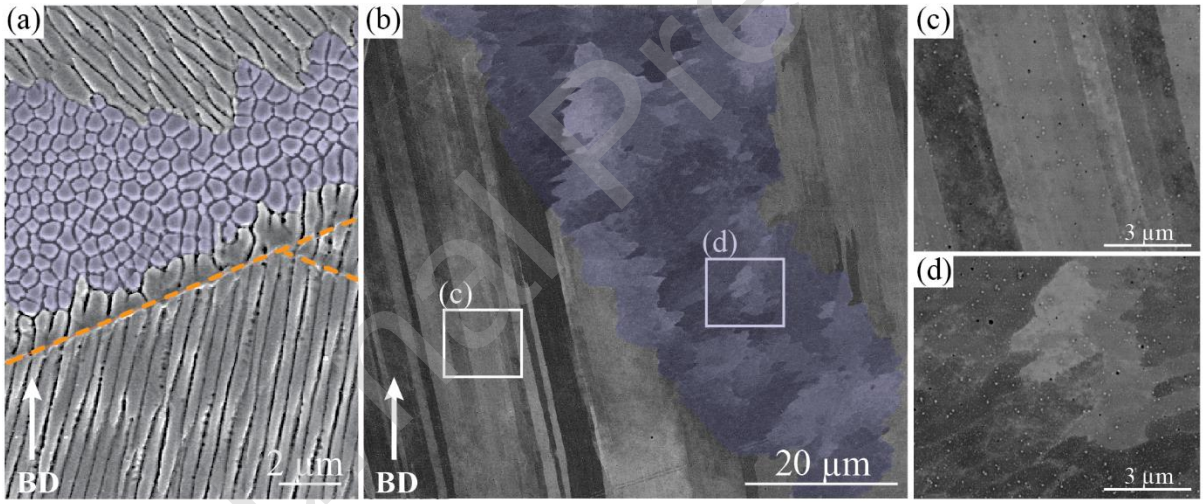

Figure 4 Side view of AB samples showing (a) SE image of an etched sample and (b) BSE imaged of a sample polished using OPS suspension. (c) and (d) are detailed views of the areas highlighted in figure (b). The cylindrical cross-sections of solidification cells cross-sectioned perpendicular to their growth direction are highlighted in blue to show the similarities between figures (a) and (b). The melt-pool border is depicted using a dashed orange line.

3.2 Microstructural characterisation of the heat-treated samples

Three different sample conditions (Table 2) were selected for mechanical testing: AB, HT1 and HT2. Heat treatment 2 (HT2) was chosen as a transition temperature between the as-built (AB) condition and heat treatment 1 (HT1). Representative microstructural features of these

samples are shown in Figure 5, showing LOM images (top row), SEM images of etched specimens (middle row) and high-resolution SEM images of non-etched specimens (bottom row). In the AB and HT2 samples, melt-pool features can be observed in both LOM and secondary electron (SE) micrographs. For the HT1 sample, the grain boundaries are etched preferentially and therefore, colour contrast is observed in the LOM and SEM images. The bottom images show backscattered electron (BSE) micrographs of unetched samples. The colour contrast in these samples originates from the preferential etching during the OPS polishing step. On the other hand, for the HT2 sample, the formation of new phases, both at intergranular and intragranular regions, is observed as indicated by the bright-coloured phases appearing in the BSE images at the bottom of Figure 5. These phases were analysed in detail by TEM as described in paragraph 3.3.

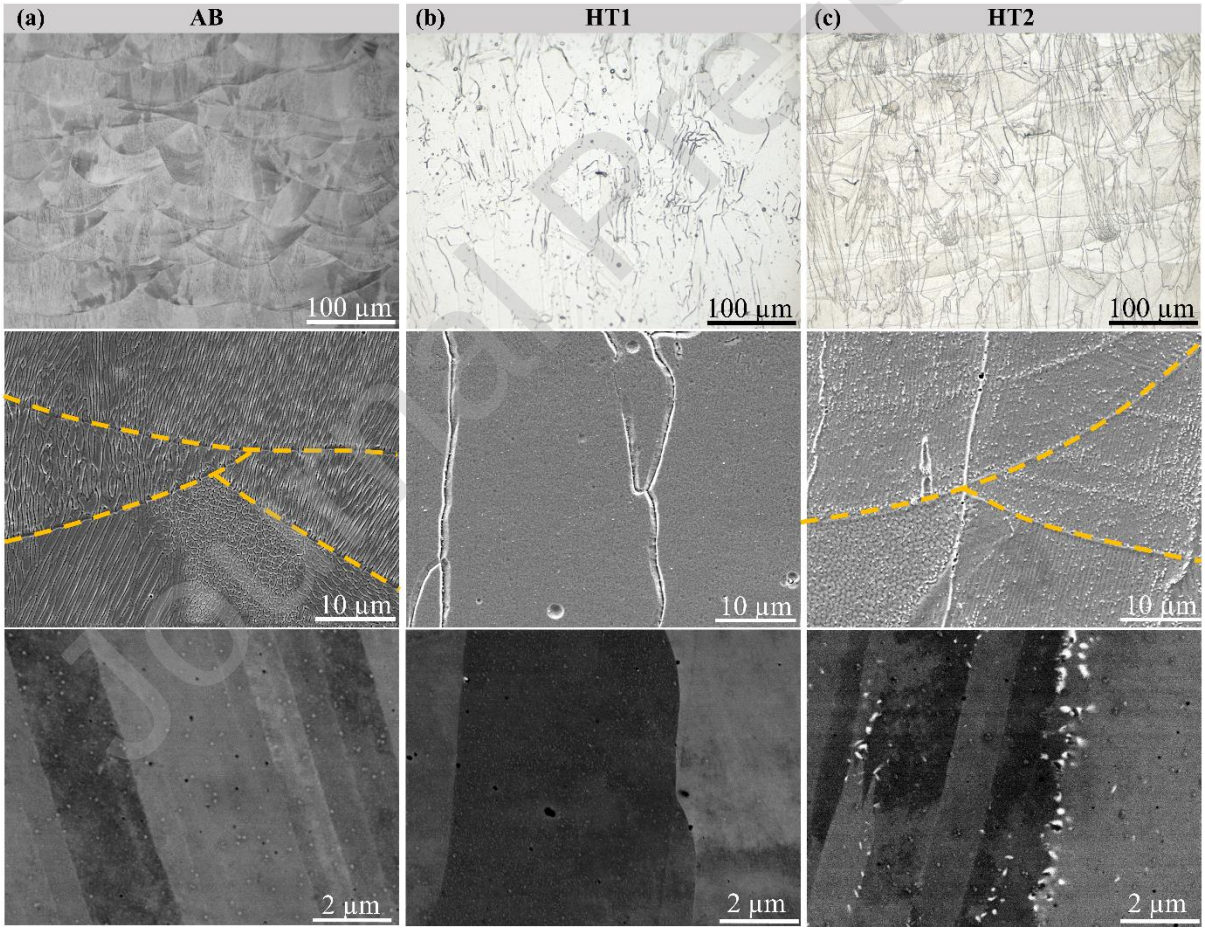

Figure 5 Microstructure from the side view for (a) AB, (b) HT1 and (c) HT2 samples. Top images are taken by LOM, middle images are SE images after etching the samples in oxalic acid and the bottom ones are BSE images after OPS polishing. The melt-pool border is depicted using dashed orange line.

The electron backscattered diffraction (EBSD) images of the three conditions (AB, HT1, HT2) were analysed in order to observe morphological and crystallographic texture differences for the three conditions. The EBSD images are shown in Figure 6 with their respective inverse pole figures (IPF) depicted along the building direction (BD). For the three sample conditions, a strong morphological texture along the building direction is observed with high aspect ratio grains. No significant grain size or grain morphology variation is observed after the heat treatments. A predominant ⟨100⟩ texture parallel to the building direction is observed for the three sample conditions. Regarding the texture index, values around 2 are observed from the IPF. An isotropic material presents a texture index of 1, therefore the samples are not highly textured along the BD. The difference between the three samples is negligible, although it should be noted that these measurements represent a local crystallographic texture.

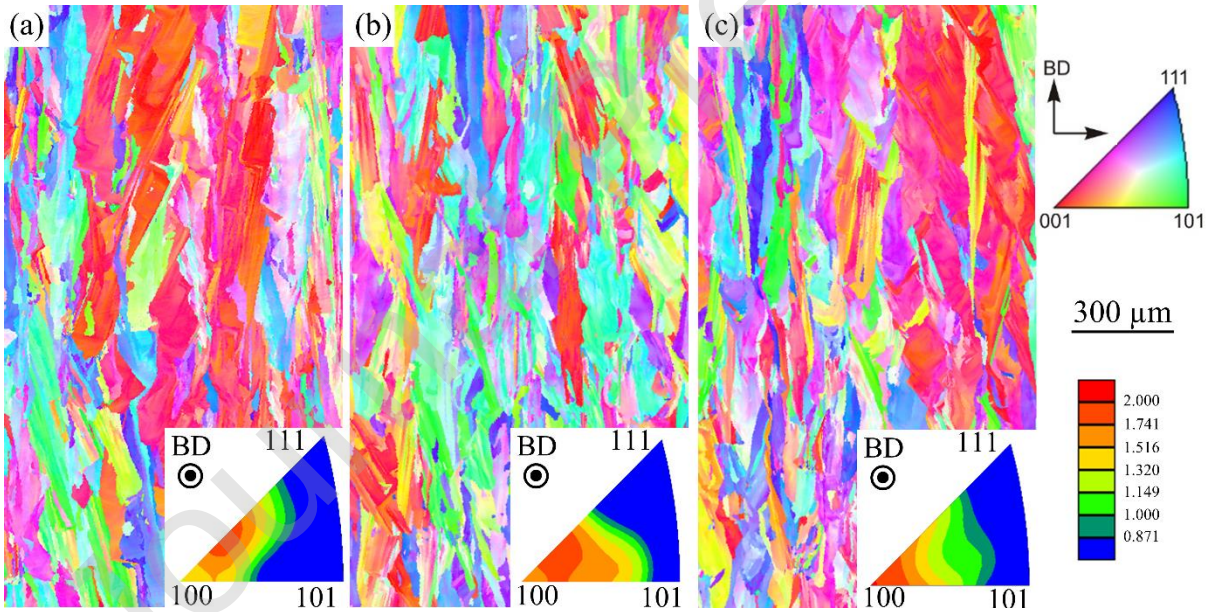

Figure 6 EBSD images of the XY plane of (a) AB, (b) HT1 and (c) HT2 samples with their respective inverse pole figures along the building direction (BD).

3.3 Transmission electron microscopy of the heat-treated samples

The sub-grain microstructure of the HT1 and HT2 samples was investigated using TEM as shown in Figure 7. For the HT1 samples, a lower dislocation density is observed as compared to the HT2 samples. The latter shows a higher dislocation density at the periphery of the cells

as well as within the cell core. No precipitates are found in the HT1 samples confirming the earlier observations done by SEM as shown in Figure 5 (b). Three different kinds of precipitates were found in the HT2 samples: two types of carbides and a Mo-rich, carbon-free phase. The two carbides are found at the grain boundaries as well as at intragranular regions. As seen in Figure 5 (c), the carbides rich in Cr and Mo as measured by EDX can be related to $M_{23}C_6$ and M_6C types of carbides respectively, as found previously in conventional [2] and SLM processed [22,25] Hastelloy X. On the other hand, the third type of precipitate, i.e. the Mo-rich phase, does not contain carbon. Due to its small size and complex structure, it was not possible to determine its exact composition. Nevertheless, from the work of Zhao et al., a Mo-rich topologically closed-packed phase, labelled as μ phase, was observed in Hastelloy X. Further work should be carried out to fully characterise this phase.

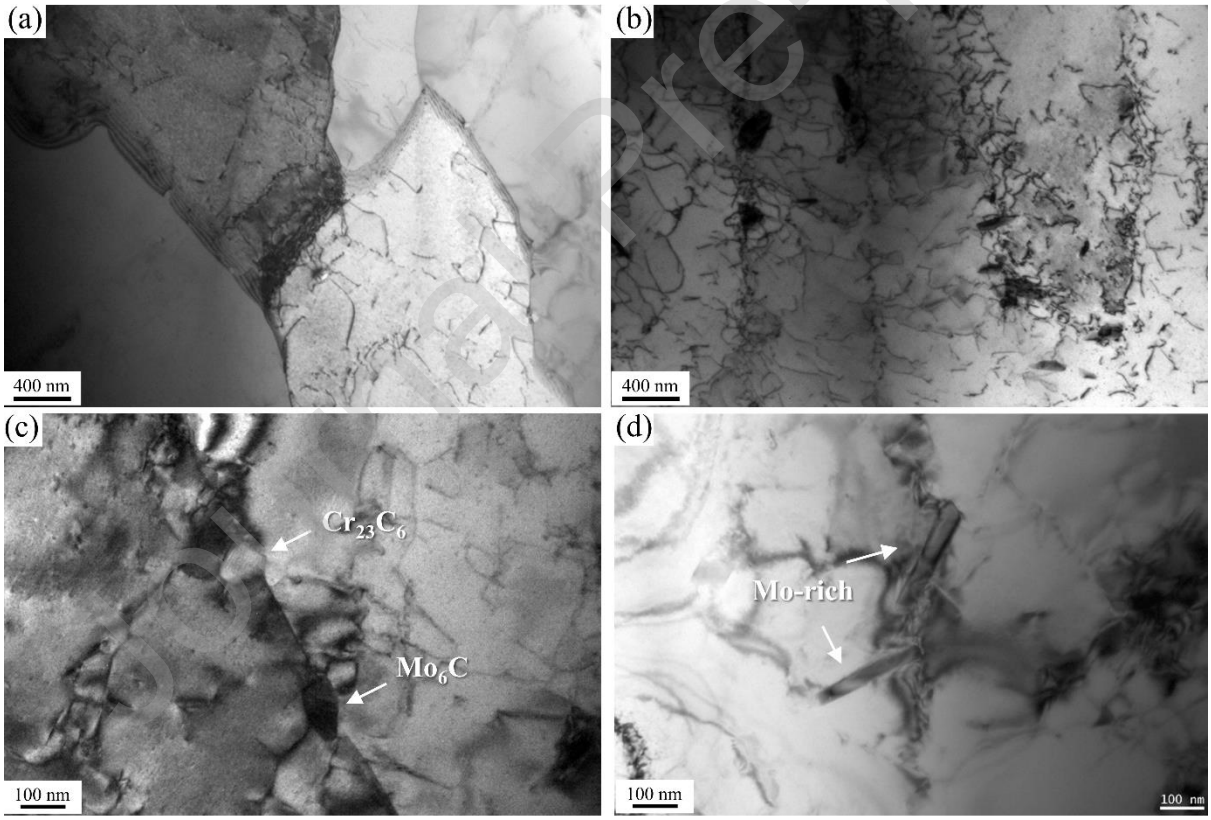

Figure 7 TEM images (a) for HT1 sample and (b,c,d) for HT2 sample. (c) shows the two type of carbides found at intergranular and intragranular regions, rich in Cr and Mo and (d) shows needle-shaped phases found within the grains rich in Mo.

3.4 High temperature tensile testing

Machined rectangular tensile specimens, built in horizontal and vertical directions, were mechanically tested at room temperature (RT), 650 °C, 750 °C and 850 °C. The yield tensile strength (YTS), ultimate tensile strength (UTS) and tensile elongation at break are depicted in Figure 8. At all testing temperatures, the YTS and UTS show similar values for the AB and HT2 samples. At room temperature, the HT1 samples show lower YTS values of around 300 MPa as opposed to yield strength values approaching 500 MPa for the AB and HT2 specimens. For all conditions, the YTS and UTS tend to decrease with increasing testing temperature independent of the applied heat treatment. At a testing temperature of 850 °C, all samples exhibit similar tensile strength values, independent on the applied heat treatment, although the HT1 samples still present slightly lower YTS and UTS values.

The tensile properties are dependent on the build orientation for the AB and HT2 samples. The horizontally-built samples present higher strength values as compared to the vertically-built samples for the AB and HT2 conditions. No difference in strength values is observed for the HT1 samples.

Different tendencies are observed for the tensile strain evolution. At all testing temperatures, the HT1 tensile samples exhibit superior strain values. Up to 650 °C, the elongation is maintained above 40% and above 30% up to a testing temperature of 850 °C. For all conditions (AB, HT1 and HT2), the strain presents a significant drop at a testing temperature of 750 °C, which is more detrimental for the AB and HT2 samples. At a testing temperature of 850 °C, an increase in elongation is observed for the AB and HT1 samples, but not for the HT2 samples. In most of the conditions, horizontally-built samples exhibit lower ductility values except for the HT1 samples, where no difference is observed between the two building directions. The tensile elongation of the AB and HT2 samples is comparable at all testing temperatures, except at 850 °C where the HT2 exhibits a lower ductility.

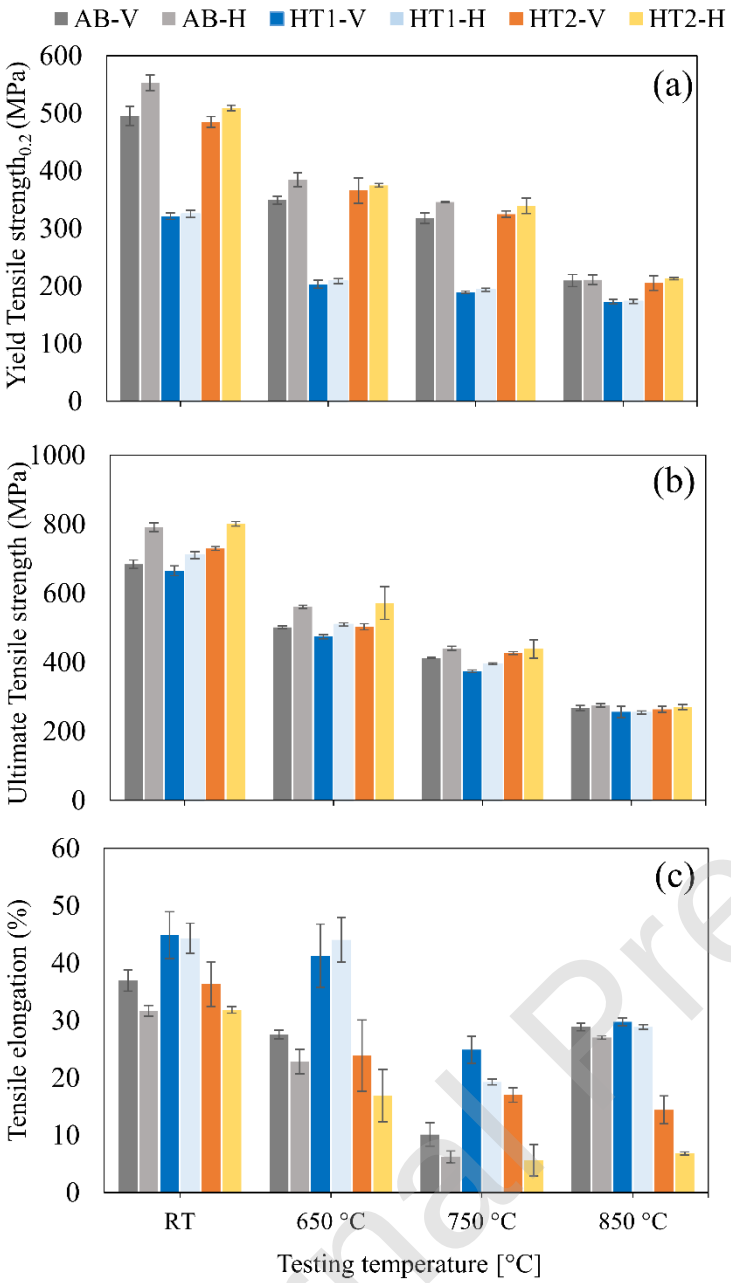

Figure 8 Tensile properties of AB, HT1 and HT2 samples built in horizontal (H) and vertical (V) direction and tested at different testing temperatures: room temperature (RT), 650 °C, 750 °C and 850 °C.

3.5 Microstructural characterisation after tensile testing

After tensile testing at elevated temperatures, the microstructure of the tested samples was analysed near the fracture surface. Figure 9 overviews the microstructures of the different tensile samples, according to their different initial states (AB, HT1 and HT2) and testing temperatures (650 °C, 750 °C and 850 °C).

After testing at 650 °C (Figure 9 (a,b,c)), no microstructural changes are observed as compared to the room temperature microstructure shown in Figure 5. When tensile testing was performed at 750 °C (Figure 9 (d,e,f)), carbides, indicated by bright spots in the BSE images, are observed at the grain boundaries within the AB and HT1 tensile samples. For all three (AB, HT1, HT2) samples tested at 750 °C, voids are observed near the grain boundaries as indicated by the regions with black contrast in the BSE images. These voids are only visible at the grain boundaries and they form around the carbides. In the case of the HT2 sample tested at 750 °C, carbides are observed both at the grain boundaries as well as within the grains.

Lastly, when tensile testing was performed at 850 °C (Figure 9 (g,h,i)), carbides are observed at the grain boundaries and within the grains for the AB samples. In addition, some needle-shaped precipitates (depicted with yellow arrows) are observed for the AB samples at intragranular regions. For the HT1 samples, only intergranular carbides are observed. In the case of the HT2 samples tested at 850 °C, a higher amount of inter- and intragranular carbides is observed as compared to the HT2 samples tested at lower testing temperatures.

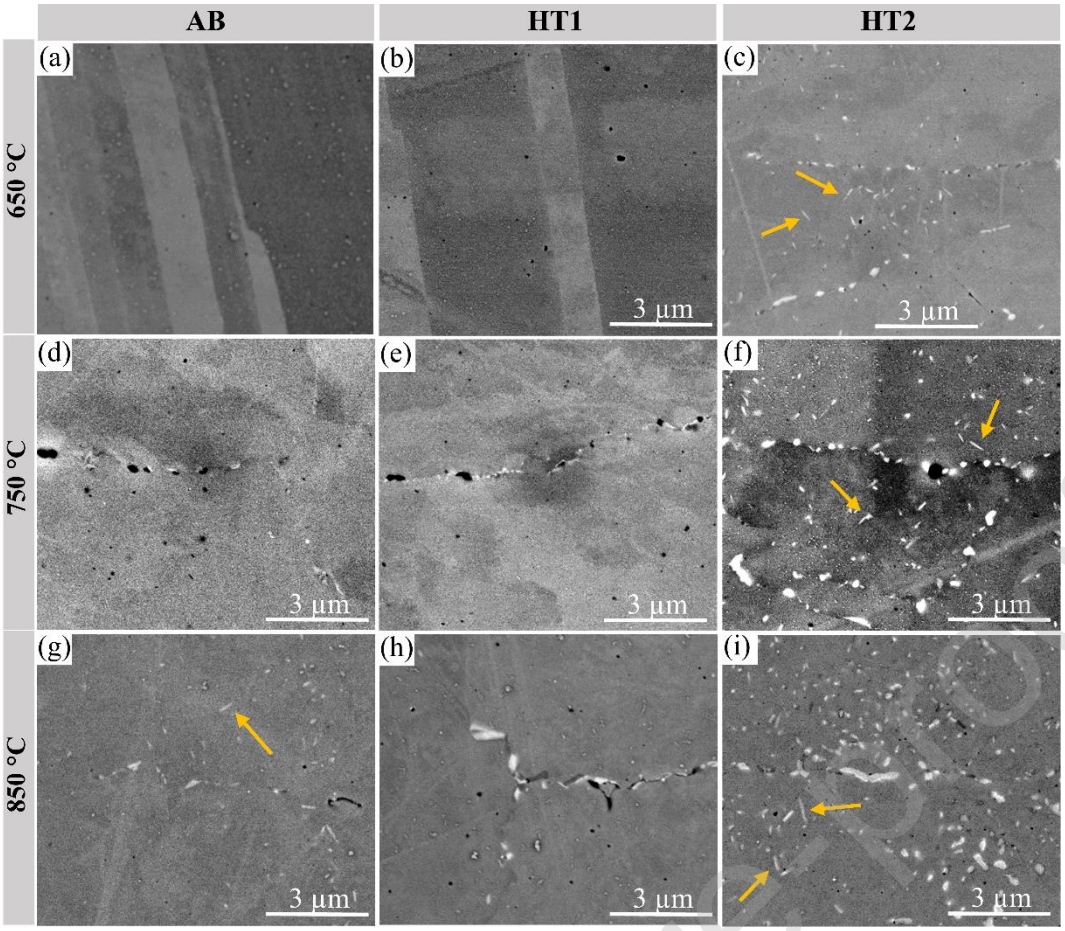

Figure 9 BSE micrographs collected from XZ cross-section of (a,d,g) AB, (b,e,h) HT1 and (c,f,i) HT2 samples after tensile testing at (a,b,c) 650 °C, (d,e,f) 750 °C and (g,h,i) 850 °C for 40 minutes followed by air cooling.

4 Discussion

In this work, the evolution of the SLM microstructure with temperature and its effect on the high-temperature tensile behaviour of micro-crack free Hastelloy X samples produced by SLM was evaluated for the first time. A standard heat treatment (1177 °C, HT1) and intermediate heat treatment (800 °C, HT2) were applied. The microstructural differences of the heat-treated samples, such as the anisotropic grain morphology, dislocation density and carbide precipitation/dissolution, were analysed. These variances were linked to the observed room temperature and high-temperature mechanical behaviour.

4.1 Room temperature tensile behaviour of micro-crack free SLM Hastelloy X

Hastelloy X is a solid-solution strengthened alloy and exhibits an age-hardening behaviour, due to carbide precipitation, when heat treated between 650 and 760 °C [4]. The standard

heat treatment applied to conventionally manufactured Hastelloy X consists of annealing at 1177 °C for 2 h and subsequent argon cooling. After thermal exposure, some carbides such as M_6C or $M_{23}C_6$ may form, as well as non-desired mu and sigma phases [2].

During SLM, the rapid solidification of Hastelloy X results in the formation of a hierarchical microstructure as observed in Figure 3 and Figure 4. Epitaxially grown grains with high aspect ratio develop along the building direction, resulting in a strong morphological texture. Within the grains, cellular sub-grains with cross-sectional diameters below 1 µm are found. As known from the literature, this cellular microstructure consists of high-density dislocation walls that act as dislocation barriers increasing the yield strength and hardness of the material significantly [7,23,26]. In Hastelloy X, M_6C carbides are considered as primary carbides since they can form during the solidification process or a thermal cycle [20,27]. In contrast to the work of Marchese et al. [20], in the current work, no M_6C carbides were observed in the AB condition.

After HT1, the samples show no visible sub-grain boundaries and no precipitates are found, neither at the grain boundaries nor within the grains. As seen in the TEM images (Figure 7), the sub-grain morphology is maintained after HT1 as previously indicated in [24]. The annealing heat treatment causes a high decrease in dislocation density as compared to the AB and HT2 samples, which is also reported in the literature [7,23]. In the current work, the HT1 samples were cooled using a forced-argon flow, attaining cooling rates above >40 °C/min to avoid the precipitation of carbides. This can be observed from the HT1 temperature profile superposed onto the time-temperature-transformation diagram (TTT) for Hastelloy X, constructed by Zhao et al. [2] (Figure 10). On the other hand, as the temperature is maintained at 800 °C for 2 h during HT2, small intergranular and intragranular carbides are observed. As shown in Figure 10, the dwell time at 800 °C for the HT2 samples leads to carbide formation despite the applied fast cooling rate from 800 °C to room temperature.

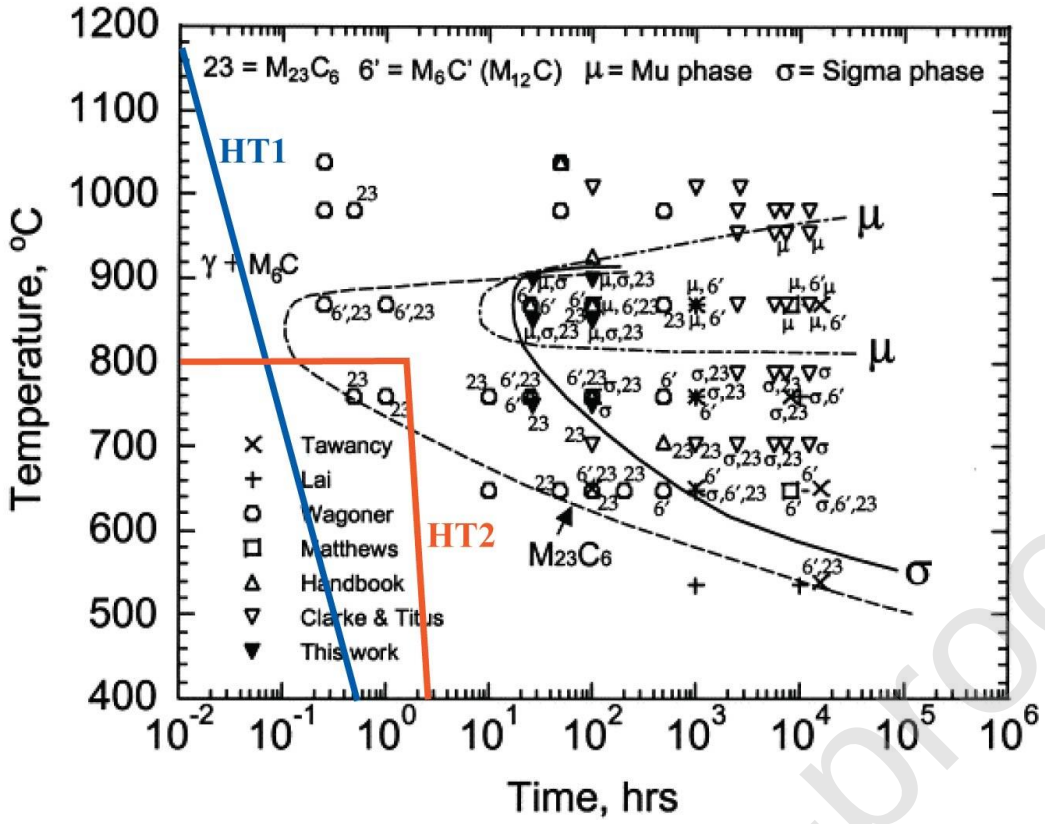

Figure 10 TTT diagram of Hastelloy X from Zhao et al. [2] *combining the two heat treatment conditions (HT1 and HT2) from this work.*

The microstructural differences between the three conditions (AB, HT1 and HT2) lead to mechanical property variations, as seen in Figure 8. For the AB samples high yield strength values are observed, which can be attributed to the high amount of dislocations at the sub-grain boundaries. In the HT2 samples, the typical SLM microstructure is still noticeable, consisting of sub-grain cells decorated with high dislocation densities as well as carbides at inter- and intradendritic regions. The combination of dislocations and carbides leads to comparable strength values to the AB samples. On the other hand, the lower dislocation density found in HT1 samples results in lower strength values than for the AB and HT2 samples. However, the HT1 sample still shows comparable values to conventional Hastelloy X (340 MPa [1]). In terms of tensile elongation values, the HT1 samples outperform the AB and HT2 samples, reaching values close to 45%. These values are comparable to the 45.5% obtained for conventionally produced Hastelloy X [1] and the SLM produced and HIPed Hastelloy X [7].

4.2 Effect of temperature on the microstructure

4.2.1 Microstructure Evolution in AB samples

The AB, HT1 and HT2 samples exhibit very different starting microstructures at room temperature. As observed in the microstructures recorded after the tensile test at elevated temperatures (Figure 9), the three heat-treated samples present different post-mortem microstructures despite experiencing the same temperature profile during tensile testing. It should be highlighted that the post-mortem microstructures shown in Figure 9 are not representative of the material during the tensile test at elevated temperatures. The microstructure is modified by the deformation during testing and changes during cooling.

In order to better understand the microstructure evolution in the AB samples during tensile testing, confocal scanning laser microscopy (CSLM) was used to mimic the temperature profile that they were subjected to. In addition, CSLM allowed monitoring the microstructural changes in situ. Figure 11 and Figure 12 show the microstructure evolution with temperature when heating up to 750 °C and 850 °C respectively, followed by a 40 minutes dwell period at the maximum temperature and subsequent fast cooling.

When the samples are heated to 750 °C, darker grain boundaries are observed at 635 °C, as seen in Figure 11 (b). At around 700 °C, the formation of a new phase at the grain boundaries is observed, indicated by the arrows. Higher colour contrast is observed between the matrix and the grain boundaries. At the onset of the dwell period at 750 °C (Figure 11 (d)), the bright-coloured grain boundaries are still present, suggesting that the carbide precipitation occurred at the grain boundaries. After 40 minutes at 750 °C (Figure 11 (e)), the bright-coloured grain boundaries are still observed but less contrast is perceived. After 40 minutes soaking time, the samples were quenched in the CSLM chamber by switching off the heating furnace, which resulted in a cooling rate of around 375 °C/min down to 300 °C and of 90

°C/min down to room temperature. These fast cooling rates assure a quenched microstructure, maintaining the high-temperature microstructure at room temperature. No significant colour contrast is perceived between the matrix and the grain boundaries at room temperature.

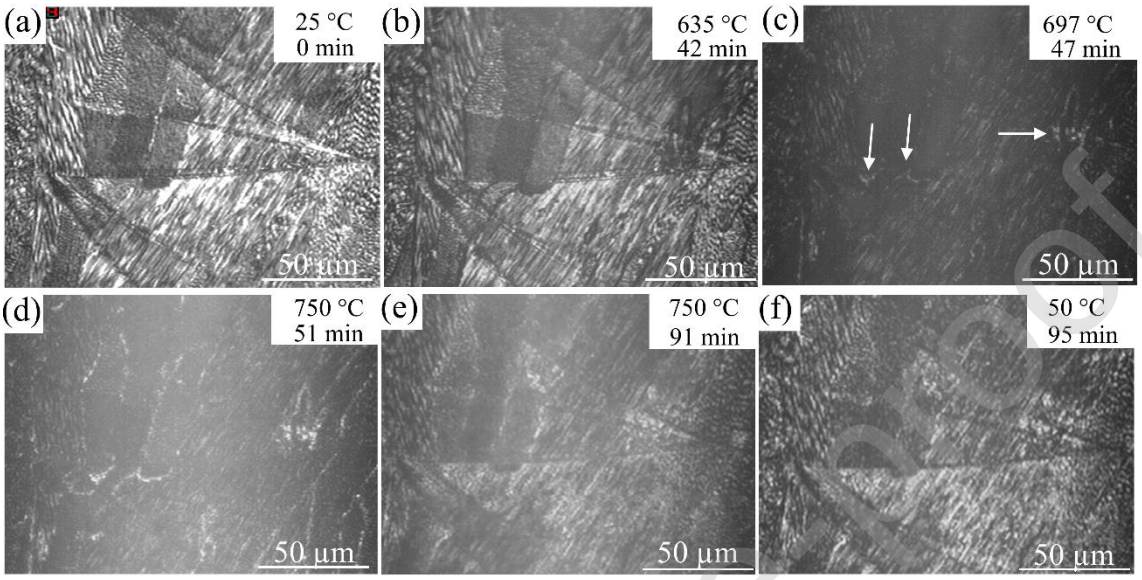

Figure 11 CSLM images from the XZ plane showing the microstructural evolution of AB samples during a typical tensile test at 750 °C. The time shown in each figure refers to the cumulative time. Notice the formation of a new phase at around 700 °C indicated with arrows in (c).

Similar effects were observed for the sample heated up to 850 °C in the CSLM, with slight variations for the temperatures at which the earlier described phase transformations occurred. At 629 °C (Figure 12(b)) darker grain boundaries are observed. At 701 °C (Figure 12(c)), precipitation of bright phases at the grain boundaries is observed (pointed out with the arrows). The precipitates remain visible up to 850 °C. After 40 minutes at 850 °C, the colour contrast between the grain boundaries and the matrix decreases. Lastly, after cooling to room temperature (Figure 12(f)), no significant colour contrast between the matrix and the grain boundaries is perceived.

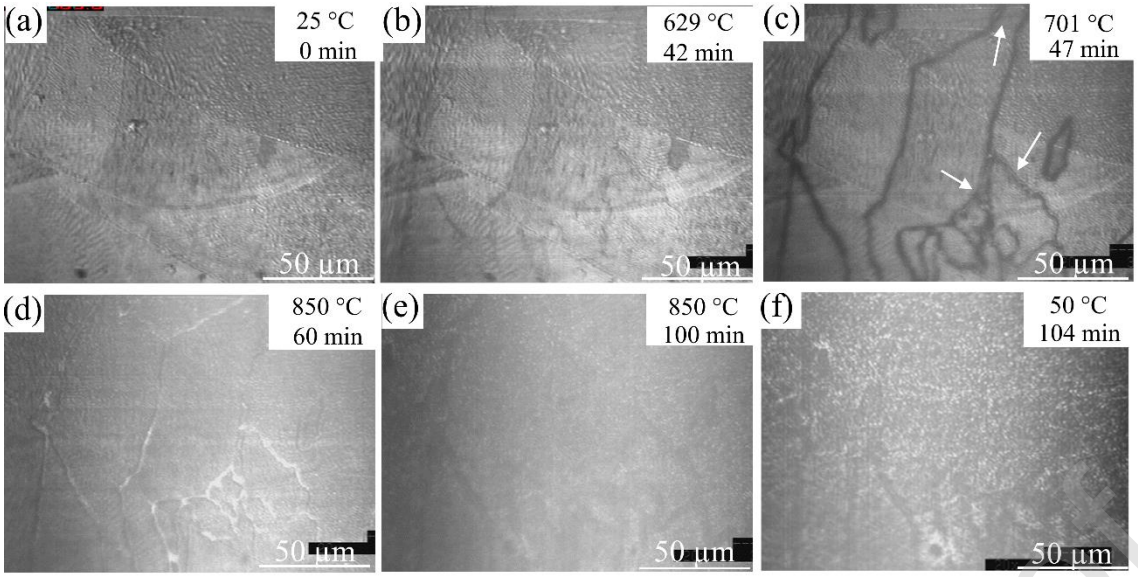

Figure 12 CSLM images from the XZ plane showing the microstructural evolution of AB samples during a typical tensile test at 850 °C. The time shown in each figure refers to the cumulative time. Notice the formation of a new phase at around 710 °C indicated with arrows in (c).

Despite the limited resolution of the optical microscope in CSLM, the images recorded at both testing temperatures indicate the onset of a phase formation initiating at around 700 °C. In order to further investigate the effect of temperature, the microstructure of the samples heated in the CSLM was analysed. The cross-sectional microstructure, originating from the centre of both CSLM samples, was further investigated, as shown in Figure 13. After holding the temperature for 40 minutes at 750 °C, carbide precipitation at the grain boundaries as well as within the intergranular regions was observed. This corresponds to the findings during CSLM, where the onset of carbide formation was observed at 700 °C. In addition, some needle-shaped phases (indicated by the arrows in Figure 13(a)) are seen, similar to the ones found by TEM (Figure 7). On the contrary, a significantly lower amount of carbides is observed for the CSLM test performed at 850 °C, as compared to the sample heated to 750 °C. A limited amount of globular-shaped carbides are present at certain grain boundaries. This suggests that for AB samples, a holding temperature of 40 minutes at 850 °C is sufficient to dissolve the intragranular carbides as well as the needle-shaped phases. The current CSLM experiments indicate that the AB tensile specimens contain a larger fraction of carbides and needle-shaped phase particles when tested at 750 °C. In contrast, only a limited

amount of globular carbides are present at the grain boundaries during testing at 850 °C. Therefore, a higher tensile elongation is expected in the AB samples when tested at 850 °C.

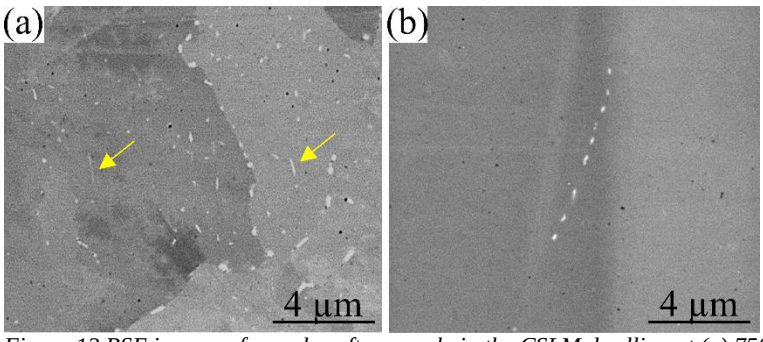

Figure 13 BSE images of samples after a cycle in the CSLM dwelling at (a) 750 °C and (b) 850 °C for 40 minutes and fast cooling.

4.2.2 Microstructure evolution in HT1 and HT2 samples

From the microstructure investigation after tensile testing (Figure 9), it was observed that the AB, HT1 and HT2 samples evolve differently after being exposed to elevated temperatures. Before tensile testing, carbides are only present in the HT2 sample. For the AB and HT1 samples, carbides start to form at the grain boundaries at a testing temperature of 750 and 850 °C. This corresponds well with the CSLM experiments performed on the AB samples. In the case of the HT2 samples, the number of carbides increases at a testing temperature of 750 and 850 °C, as compared to the AB and HT1 samples.

Overall, due to the larger fraction of carbides and the presence of a brittle needle-like phase, it is expected that the HT2 samples will exhibit less tensile elongation as compared to the HT1 samples. In addition, the HT2 samples present a cellular solidification microstructure, high dislocation density and a high amount of carbides. Therefore, it is expected that the HT2 samples will exhibit higher yield and tensile strength values than HT1 samples, independent on the testing temperature.

When comparing microstructures of as-built and heat-treated samples, it is clear that the hierarchical microstructure and the high dislocation densities obtained after SLM determine the phase formation up to 850 °C in the AB samples. In addition, based on the conventional

Hastelloy X TTT diagram shown in Figure 10, the formation of topologically closed-packed (TPC) phases like sigma or mu phases is only expected after 10 h of exposure time. In this work, needle-shaped phases were observed by TEM in the HT2 samples and the AB samples after holding them at 850 °C for 2 h and 40 min inside the CSLM, respectively. This work demonstrates that the conventional Hastelloy TTT diagrams cannot fully predict the presence of those phases.

4.3 Effect of the temperature on the mechanical properties

The high-temperature tensile tests indicated an overall decrease in UTS and YTS with increasing testing temperature. This can be attributed to the decrease in dislocation density as the samples are brought to a higher temperature. The differences between the three heat treatment conditions become more noticeable at low temperatures due to the microstructural differences. For AB samples, the high strength found is attributed to the high dislocation density within the AB samples. For HT2 samples, the incomplete annihilation of dislocations and carbide precipitation results in the high yield strength values. At 850 °C, the microstructural differences between AB, HT1 and HT2 samples are reduced, resulting in similar tensile strength values for all the three heat treatments.

4.3.1 Tensile elongation variations

With respect to the tensile elongation, however, a continuous decrease is observed for all the samples up to 750 °C. Tomus et al. [19] also reported a reduction in the tensile strain elongation at 700 °C and 900 °C of Hastelloy X processed by SLM. Using CSLM, the temperature at which carbides started to form was defined as 700 °C. The presence of carbides increases the strength of the material, but due to their brittle nature, they can reduce the tensile elongation. Tawacy et al. [4] observed a decrease in strain due to the formation of a continuous film of carbides at the grain boundaries of Hastelloy X when ageing at

temperatures above 760 °C. Therefore, the significant decrease in elongation observed for samples tested at 750 °C is explained by the carbide precipitation at the grain boundaries and within the grains. On the other hand, void formation is also observed at grain boundaries and close to the carbides, after tensile testing at elevated temperatures. This again confirms the relationship between the presence of carbide precipitates and the decrease in ductility.

During high-temperature exposure, carbon tends to segregate to high dislocation-density regions, stacking faults and grain boundaries, leading to carbide precipitation sites [4]. As the dislocation density is higher in the AB and HT2 samples, as compared to the HT1 samples, carbide precipitation is more likely to occur in the former samples. These differences can explain the elongation variances observed for the two conditions when testing at 750 °C, where the AB samples exhibit much lower tensile ductility, similar to the values obtained for the HT2 samples.

Although the AB, HT1 and HT2 samples follow the same trend with respect to the elongation strain, they differ slightly in the amount of strain recovery at 850 °C. The AB and HT1 samples exhibit an increase in elongation from 750 to 850 °C. This increase is explained by the carbide dissolution observed by CSLM for the AB samples when heating to 850 °C. The increase in elongation was not, however, found for the HT2 samples. The starting microstructure of the HT2 samples contains a high amount of precipitates, both at intergranular and intragranular regions. During tensile testing at 750 and 850 °C, both the amount and size of carbides and needle-shaped phases grew in population and size. Therefore, the 40 minutes holding time at 850 °C was not sufficient for their complete dissolution (Figure 9 (c)).

4.3.2 Anisotropy of mechanical properties

Anisotropy was observed in the mechanical performance at all the testing temperatures for the AB and HT2 samples. The horizontally-built samples present higher strength values than the vertically-built samples. The tensile elongation values show the opposite tendency. From the literature, similar trends were observed by Tomus et al. [23] when testing in both directions for Hastelloy X produced by SLM. For CoCr [28] and In738LC [10], similar trends were observed when comparing the tensile properties of horizontally and vertically-built specimens. In contrast, the HT1 samples do not exhibit a very pronounced directional dependency, especially with respect to the yield strength.

When increasing the tensile testing temperature, the difference in mechanical performance between horizontally and vertically built samples is significantly decreased for all samples. The combination of morphological and crystallographic texture might cause this anisotropic behaviour. In the horizontally-built samples, the number of grain boundaries perpendicular to the tensile loading direction and the number of grain boundary carbides is larger, so higher strength values and lower ductility values can be expected.

5 Conclusions

In this work, the microstructure and mechanical property evolution of micro-crack free Hastelloy X parts produced by SLM using a commercial powder upon exposure at elevated temperatures has been studied for the first time.

The samples were tested at elevated temperature in three different states: as-built (AB), heat-treated at 1177 °C (HT1) and heat-treated at 800 °C (HT2). Based on EBSD scans recorded at low magnification, no significant changes in the fcc matrix grain size nor their morphology was observed, when the three conditions were compared. The HT2 heat-treated samples

contained carbides at intergranular and transgranular regions. HT1 heat-treated samples did not contain carbides and a smaller amount of dislocations.

The high-temperature tensile tests indicated a decrease in yield and ultimate tensile strength for all conditions when the testing temperature was increased. A significant decrease in elongation was observed when tensile testing was performed at 750 °C. This was attributed to the carbide formation at the grain boundaries independent on the initial microstructure of the test specimens. When the samples underwent HT1, which is a standard heat treatment for Hastelloy X, however, the lowest decay in elongation was observed during the tensile testing at 750 °C. As the initial microstructure of HT1 samples contained a lower dislocation density and a more homogeneous microstructure as compared to AB samples, it is suggested that less favourable carbide nucleation sites are present in the HT1 samples. In addition, HT1 samples exhibit the highest ductility values, independent of the testing conditions.

Confocal Scanning Laser Microscopy (CSLM) tests allowed to visualise the microstructure evolution mimicking the temperature profile that the AB tensile samples experienced when testing at 750 and 850 °C. At 700 °C, carbide formation initiated at grain boundaries. The formed carbides were stable up to 750 and 850 °C. However, when holding the temperature for 40 minutes at 850 °C, carbide dissolution was observed explaining the ductility increase seen for AB samples tested at 850 °C.

Declarations of interest: none

Acknowledgements

This research was supported by the ENGIE Research and Technology Division. The authors acknowledge ENGIE Research and Technology Division for the use of the SLM280HL machine and Oerlikon for the advice in the Hastelloy X powder variant selection and heat treatment.

References

[1] Haynes-International, Hastelloy X Alloy, High-Temperature Alloy. 06002 (1997) 16.

[2] J.-C. Zhao, M. Larsen, V. Ravikumar, Phase precipitation and time–temperature-transformation diagram of Hastelloy X, Mater. Sci. Eng. A. 293 (2000) 112–119. doi:10.1016/S0921-5093(00)01049-2.

[3] H. Kirchhöfer, F. Schubert, H. Nickel, Precipitation Behavior of Ni–Cr–22 Fe–18 Mo (Hastelloy-X) and Ni-Cr-22 Co-12 Mo (Inconel-617) After Isothermal Aging, Nucl. Technol. 66 (2017) 139–148. doi:10.13182/NT84-A33462.

[4] H.M. Tawancy, Long-term ageing characteristics of Hastelloy alloy X, J. Mater. Sci. 18 (1983) 2976–2986. doi:10.1007/BF00700780.

[5] J.-P. Kruth, G. Levy, F. Klocke, T.H.C. Childs, Consolidation phenomena in laser and powder-bed based layered manufacturing, CIRP Ann. - Manuf. Technol. 56 (2007) 730–759. doi:10.1016/j.cirp.2007.10.004.

[6] ASTM, Standard Terminology for Additive Manufacturing Technologies ASTM F2792–10, 2015.

[7] M.L. Montero-Sistiaga, S. Pourbabak, J. Van Humbeeck, D. Schryvers, K. Vanmeensel, Microstructure and mechanical properties of Hastelloy X produced by

HP-SLM (high power selective laser melting), Mater. Des. 165 (2019) 107598. doi:10.1016/j.matdes.2019.107598.

[8] B. Vrancken, V. Cain, R. Knutsen, J. Van Humbeeck, Residual stress via the contour method in compact tension specimens produced via selective laser melting, Scr. Mater. 87 (2014) 29–32. doi:10.1016/j.scriptamat.2014.05.016.

[9] A.H. Nickel, D.M. Barnett, F.B. Prinz, Thermal stresses and deposition patterns in layered manufacturing, Mater. Sci. Eng. A. 317 (2001) 59–64. doi:10.1016/S0921-5093(01)01179-0.

[10] L. Rickenbacher, T. Etter, S. Hövel, K. Wegener, High temperature material properties of IN738LC processed by selective laser melting (SLM) technology, Rapid Prototyp. J. 19 (2013) 282–290. doi:10.1108/13552541311323281.

[11] M. Cloots, P.J. Uggowitzer, K. Wegener, Investigations on the microstructure and crack formation of IN738LC samples processed by selective laser melting using Gaussian and doughnut profiles, Mater. Des. 89 (2016) 770–784. doi:10.1016/j.matdes.2015.10.027.

[12] S. Catchpole-Smith, N. Aboulkhair, L. Parry, C. Tuck, I.A. Ashcroft, A. Clare, Fractal scan strategies for selective laser melting of 'unweldable' nickel superalloys, Addit. Manuf. 15 (2017) 113–122. doi:10.1016/J.ADDMA.2017.02.002.

[13] L.N. Carter, C. Martin, P.J. Withers, M.M. Attallah, The influence of the laser scan strategy on grain structure and cracking behaviour in SLM powder-bed fabricated nickel superalloy, J. Alloys Compd. 615 (2014) 338–347. doi:10.1016/j.jallcom.2014.06.172.

[14] V.D. Divya, R. Muñoz-Moreno, O.M.D.M. Messé, J.S. Barnard, S. Baker, T. Illston,

H.J. Stone, Microstructure of selective laser melted CM247LC nickel-based superalloy and its evolution through heat treatment, Mater. Charact. 114 (2016) 62–74. doi:10.1016/J.MATCHAR.2016.02.004.

[15] K.-T. Hsu, H.-S. Wang, H.-G. Chen, P.-C. Chen, Effects of the Hot Isostatic Pressing Process on Crack Healing of the Laser Repair-Welded CM247LC Superalloy, Metals (Basel). 6 (2016) 238. doi:10.3390/met6100238.

[16] F. Wang, Mechanical property study on rapid additive layer manufacture Hastelloy® X alloy by selective laser melting technology, Int. J. Adv. Manuf. Technol. 58 (2012) 545–551. doi:10.1007/s00170-011-3423-2.

[17] D. Tomus, T. Jarvis, X. Wu, J. Mei, P. Rometsch, E. Herny, J.F. Rideau, S. Vaillant, Controlling the microstructure of Hastelloy-X components manufactured by Selective Laser Melting, Phys. Procedia. 41 (2013) 823–827. doi:10.1016/j.phpro.2013.03.154.

[18] N.J. Harrison, I. Todd, K. Mumtaz, Reduction of micro-cracking in nickel superalloys processed by Selective Laser Melting: A fundamental alloy design approach, Acta Mater. 94 (2015) 59–68. doi:10.1016/j.actamat.2015.04.035.

[19] D. Tomus, P.A. Rometsch, M. Heilmaier, X. Wu, Effect of minor alloying elements on crack-formation characteristics of Hastelloy-X manufactured by selective laser melting, Addit. Manuf. 16 (2017) 65–72. doi:10.1016/J.ADDMA.2017.05.006.

[20] G. Marchese, G. Basile, E. Bassini, A. Aversa, D. Ugues, P. Fino, S. Biamino, Study of the Microstructure and Cracking Mechanisms of Hastelloy X Produced by Laser Powder Bed Fusion, Materials (Basel). 11 (2018) 106. doi:10.3390/ma11010106.

[21] O. Sanchez-Mata, X. Wang, J.A. Muñiz-Lerma, M.A. Shandiz, R. Gauvin, M. Brochu, M. Attarian Shandiz, R. Gauvin, M. Brochu, Fabrication of crack-free nickel-based

superalloy considered non-weldable during laser powder bed fusion, Materials (Basel). 11 (2018) 1–9. doi:10.3390/ma11081288.

[22] G. Marchese, E. Bassini, A. Aversa, M. Lombardi, D. Ugues, P. Fino, S. Biamino, Microstructural Evolution of Post-Processed Hastelloy X Alloy Fabricated by Laser Powder Bed Fusion, Materials (Basel). 12 (2019) 486. doi:10.3390/ma12030486.

[23] D. Tomus, Y. Tian, P.A.P.A.P.A. Rometsch, M. Heilmaier, X. Wu, Influence of post heat treatments on anisotropy of mechanical behaviour and microstructure of Hastelloy-X parts produced by selective laser melting, Mater. Sci. Eng. A. 667 (2016) 42–53. doi:10.1016/j.msea.2016.04.086.

[24] S. Pourbabak, M.L. Montero-Sistiaga, D. Schryvers, J. Van Humbeeck, K. Vanmeensel, Microscopic investigation of as built and hot isostatic pressed Hastelloy X processed by Selective Laser Melting, Mater. Charact. 153 (2019) 366–371. doi:10.1016/J.MATCHAR.2019.05.024.

[25] D. Tomus, Y. Tian, P.A. Rometsch, M. Heilmaier, X. Wu, Influence of post heat treatments on anisotropy of mechanical behaviour and microstructure of Hastelloy-X parts produced by selective laser melting, Mater. Sci. Eng. A. 667 (2016) 42–53. doi:10.1016/J.MSEA.2016.04.086.

[26] Y. Zhong, L. Liu, S. Wikman, D. Cui, Z. Shen, Intragranular cellular segregation network structure strengthening 316L stainless steel prepared by selective laser melting, J. Nucl. Mater. 470 (2016) 170–178. doi:10.1016/j.jnucmat.2015.12.034.

[27] G. Bai, J. Li, R. Hu, T. Zhang, H. Kou, H. Fu, Effect of thermal exposure on the stability of carbides in Ni–Cr–W based superalloy, Mater. Sci. Eng. A. 528 (2011) 2339–2344. doi:10.1016/J.MSEA.2010.11.088.

[28] H.W. Lee, K.-H. Jung, S.-K. Hwang, S.-H. Kang, D.-K. Kim, Microstructure and mechanical anisotropy of CoCrW alloy processed by selective laser melting, Mater. Sci. Eng. A. 749 (2019) 65–73. doi:10.1016/J.MSEA.2019.02.013.